ARL-TR-8313 ● MAR 2018

US Army Research Laboratory

Convergence of Ground and Excited State Properties of Divacancy Defects in 4H-SiC with Computational Cell Size

by Ariana Beste and DeCarlos E Taylor

NOTICES

Disclaimers

The findings in this report are not to be construed as an official Department of the Army position unless so designated by other authorized documents.

Citation of manufacturer's or trade names does not constitute an official endorsement or approval of the use thereof.

Destroy this report when it is no longer needed. Do not return it to the originator.

ARL-TR-8313 ● MAR 2018

US Army Research Laboratory

Convergence of Ground and Excited State Properties of Divacancy Defects in 4H-SiC with Computational Cell Size

by Ariana Beste
Oak Ridge Associated Universities, Belcamp, MD

DeCarlos E Taylor
Weapons and Materials Research Directorate, ARL

REPORT DOCUMENTATION PAGE

Form Approved
OMB No. 0704-0188

1. REPORT DATE *(DD-MM-YYYY)*	2. REPORT TYPE	3. DATES COVERED (From - To)
March 2018	Technical Report	October 2017–October 2018

4. TITLE AND SUBTITLE
Convergence of Ground and Excited State Properties of Divacancy Defects in 4H-SiC with Computational Cell Size

5a. CONTRACT NUMBER

5b. GRANT NUMBER

5c. PROGRAM ELEMENT NUMBER

6. AUTHOR(S)
Ariana Beste and DeCarlos E Taylor

5d. PROJECT NUMBER
W911NF-17-2-0040

5e. TASK NUMBER

5f. WORK UNIT NUMBER

7. PERFORMING ORGANIZATION NAME(S) AND ADDRESS(ES)
US Army Research Laboratory
ATTN: RDRL-WML-B
Aberdeen Proving Ground, MD 21005-5069

8. PERFORMING ORGANIZATION REPORT NUMBER
ARL-TR-8313

9. SPONSORING/MONITORING AGENCY NAME(S) AND ADDRESS(ES)

10. SPONSOR/MONITOR'S ACRONYM(S)

11. SPONSOR/MONITOR'S REPORT NUMBER(S)

12. DISTRIBUTION/AVAILABILITY STATEMENT
Approved for public release; distribution is unlimited.

13. SUPPLEMENTARY NOTES

14. ABSTRACT
Deep defect centers in semiconductors show electronic behavior that can be exploited in quantum computing applications. In particular, the neutral divacancy defect in 4H-SiC has been considered as a potential qubit material that is individually addressable in the near IR. To study the divacancy defect computationally, the behavior of properties relevant to the function of the material as a qubit with respect to computational parameters needs to be established. We used density functional theory to compute defect formation energies of the neutral and charged *hh* divacancy with corresponding charge transition levels, the position of the highest occupied, localized defect state within the band gap, and excitation energies for the ^{3}A to ^{3}E transition (absorption, zero phonon lines, and emission), which is essential for optical initialization and read-out. We investigated the convergence of these properties with respect to computational cell size and studied the effects of lattice relaxation and dispersion corrections. Based on our results, we recommend computational parameters for future computational work.

15. SUBJECT TERMS
density functional theory, PBE, defect formation energy, charge transition levels, absorption, zero phonon lines, emission

16. SECURITY CLASSIFICATION OF:			17. LIMITATION OF ABSTRACT	18. NUMBER OF PAGES	19a. NAME OF RESPONSIBLE PERSON
a. REPORT	b. ABSTRACT	c. THIS PAGE			Ariana Beste
Unclassified	Unclassified	Unclassified	UU	44	19b. TELEPHONE NUMBER (Include area code) 410-306-4735

Contents

List of Figures

List of Tables

Acknowledgments

This work was funded by the Department of Defense and conducted at the US Army Research Laboratory (ARL). It was supported in part by a grant of computer time from the Department of Defense High Performance Computing Modernization Program at the US Army Research Laboratory Supercomputing Resource Center. Ariana Beste was sponsored by ARL under Cooperative Agreement Number W911NF-17-2-0040. The views and conclusions contained in this document are those of the authors and should not be interpreted as representing the official policies, either expressed or implied, of ARL or the US government. The US government is authorized to reproduce and distribute reprints for government purposes notwithstanding any copyright notation herein.

1. Introduction

Qubits, units of quantum information, have been realized in various systems; for instance, in electrons floating on liquid helium,[1,2] nuclear spin states of liquids,[3] spin states of quantum dots coupled to superconductors,[4,5] and rare-earth-doped solids.[6,7] A requirement for a functioning qubit is that it maintains its quantum state for a long time (at least until read-out) and should, therefore, be isolated from its environment and unwanted external fluctuations. However, complete isolation is undesired since it would not allow for spin entanglement that is a prerequisite to perform quantum manipulations. Isolated atoms possess well-defined quantum states and have been used to fabricate a general-purpose 5-qubit quantum computer.[8] However, the incorporation of atoms in devices requires ion traps or optical lattices. Point defects in semiconductors or insulators can exhibit behavior similar to atoms and have been shown to be suitable for quantum computing applications.[9,10] Electronic states of deep defect centers are composed of atomic orbitals of neighboring atoms that are localized and typically found within, or close to, the band gap. A prototypical, well-studied example of a deep center and promising candidate qubit material is the diamond nitrogen vacancy (NV).[11–13] While the diamond NV is individually addressable and can be initialized, manipulated, and measured at room temperature,[12] it is difficult to manufacture diamond devices on a large scale.

A technologically advanced material that is used in semiconductor electronic devices is silicon carbide (SiC). It can be grown in large single crystals, has a wide band gap,[14] can either be p- or n-type doped, exhibits small spin-orbit coupling,[15] and has zero nuclear spin in its most common isotopes. A variety of stable defects such as monovacancies, divacancies, antisites, NV centers, and defect combinations have been identified in SiC[16–18] and considered as potential qubit materials.[19] The wealth of polytypes that exist in SiC provides the possibility of tuning the location of the defect energy levels within the band gap for qubit applications.[9,10] The more common polytypes are 4H, 6H, and 3C.

Here, we focus on the neutral divacancy in 4H-SiC that has been shown to be individually addressable in the near IR.[20] The localized triplet ground state of the defect can be optically spin polarized similar to the diamond NV center[10] and is schematically shown in Fig. 1. The $m_S = 0$ and –1 spin sublevels of the ^3A state can function as the qubit states. Optical initialization proceeds through a spin-conserving transition from the ^3A to the ^3E state followed by a spin-selective nonradiative decay to an intermediate ^1A state that allows optical pumping into the $m_S = 0$ sublevel of the ^3A ground state. After initialization, the qubit states can be coherently manipulated with pulsed microwaves, and their spin-state can be read

out by spin-dependent measurement of the photoluminescence intensity after electronic excitation.[21] The photoluminescence spectra of the divacancy in 4H-SiC display 4 distinct zero phonon lines (ZPLs)[21] stemming from the 4 possible divacancy configurations depicted in Fig. 2. The measured ZPLs correspond to the transition between the ^{3}A state and the structurally relaxed ^{3}E state, as displayed in Fig. 3.

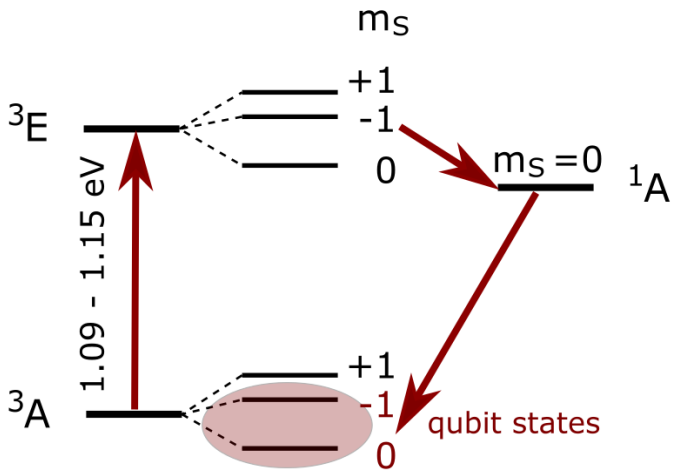

Fig. 1 Schematic representation of the optical initialization of the qubit states for the neutral divacancy defect in 4H-SiC (transition energies from Shi et al.[1])

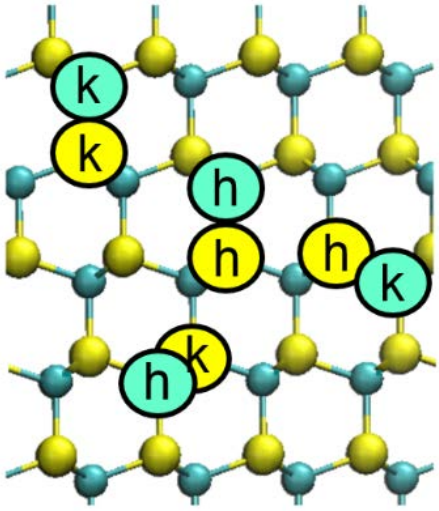

Fig. 2 Four inequivalent forms of the divacancy defect in 4H-SiC, *hh* and *kk* axial divacancies, *hk* and *kh* basal divacancies; carbon = teal, silicon = yellow

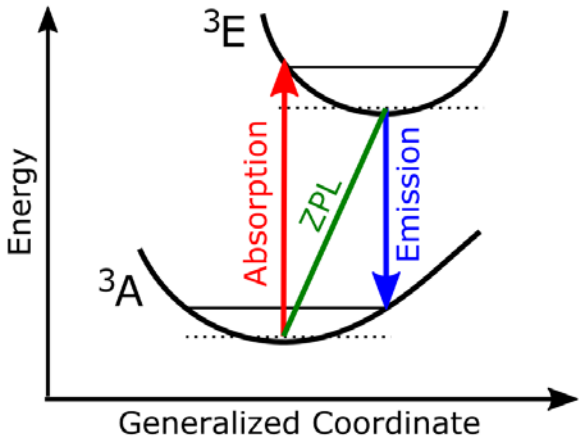

Fig. 3 Configuration coordinate diagram for the ^{3}A to ^{3}E transition indicating adiabatic ZPL, vertical absorption, and vertical emission lines

The majority of prior computational work on defects in 4H-SiC has been focused on ground state properties. In particular, the calculation of hyperfine tensors enables comparison between computational and electron paramagnetic resonance results facilitating experimental assignment.[16–18,22–26] Defect formation energies as a function of the Fermi level and charge state transition levels have been computed[19,22, 26–30] to determine which charge states are likely to form. In that work, a wide range of computational cell sizes have been used, ranging from cells containing 96–576 atoms. The calculations have been carried out utilizing the local density or generalized gradient approximation (GGA), with some studies[19,26,27] employing a more computationally demanding hybrid functional. Depending on system and property studied, pure density functionals can introduce large errors due to the underestimation of the band gap. For instance, for the negatively charged carbon vacancy it has been reported that the application of pure density functionals leads to an incorrect ground state.[26] For interstitials and single vacancies in 3C-SiC, it was found that pure density functionals under- or over-estimate defect formation energies depending on the charge state.[31] Nonsystematic errors as a function of the charge state lead to shifts in the charge transition levels, which has been observed for the divacancy in 4H-SiC to be 0.5 eV.[27]

Calculated ZPLs for defects in 4H-SiC have been reported to a lesser extent. The NV center in 4H-SiC shows properties similar to the analogous defect in diamond but with a smaller ZPL for the triplet-triplet transition.[10,19,32,33] ZPLs have been calculated for the neutral divacancy defect using the constrained density functional theory (DFT) approach.[32,34] Again, the under-estimation of the band gap with pure density functionals is a potential source of error since localized acceptor states originating at the defect may incorrectly interact with states in the conduction band or may be erroneously located above the conduction band edge. As a partial

remedy, hybrid functionals were used in the calculation of ZPLs of divacancy defects employing small computational cells of 96 atoms,[10,34] where the achieved accuracy was reported to be within 0.1 eV[34] based on comparison of computed ZPLs with experiment results. Furthermore, ZPL calculations were carried out[32] with a computational cell containing 432 atoms and a hybrid functional. Since a cell of this size is very resource-intensive when using hybrid functionals, computational parameters were chosen to minimize computational demands (small energy cutoff for norm-conserving pseudopotentials, GGA geometries). Alternatively, the excitation spectrum of the neutral divacancy has been studied with time-dependent DFT,[35] albeit within a finite cluster approximation.

If inaccuracies of standard GGA functionals necessitate the application of hybrid functionals, or even many-body techniques such as the GW method for excitation spectra, then the practical size limit for the computational cell is comparatively small. However, if supercells are chosen that result in errors due to finite size effects that are larger than the errors introduced by the level of theory, it is not sensible to perform calculations at high levels of sophistication. Focusing on the *hh* divacancy in 4H-SiC, in this work we explore the effect of computational cell size on defect properties relevant to the exploitation of the defect for qubit applications. We use standard GGA to examine large systems with the expectation that the results are transferrable to other DFT functionals. We also probe the computational cell-size dependence of the highest occupied Kohn-Sham defect state, which gives a first indication of the cell size needed for GW approaches.

2. Computational Methods

All computation were performed with the Quantum Espresso[36] (QE) program package. We employed the Perdew-Burke-Ernzerhof (PBE) functional[37] within DFT and a Martins-Troullier norm-conserving pseudopotential available on the QE webpage. We tested convergence behavior with and without the Grimme D2 dispersion correction.[38,39] A kinetic energy cutoff of 70 Ry was used, which yields a 0.001% total energy deviation relative to the energy of 4H-SiC calculated with a 552-cell expansion (400 atoms), a 2 × 2 × 2 Monkhorst-Pack k-point mesh, and an 80-Ry cutoff.

The cell expansions generated in this work were derived from the 8-atom hexagonal unit cell for bulk 4H-SiC with ABCB stacking, shown in Fig. 4. The Monkhorst-Pack k-point mesh employed depends on the cell size and is given in Table 1. Variations in bulk lattice parameters due to differing cell expansions and k-point grids, were below 10^{-3} Å. Calculated lattice parameters were 3.069 Å, 10.060 Å and 3.087 Å, 10.105 Å, respectively, with and without dispersion correction.

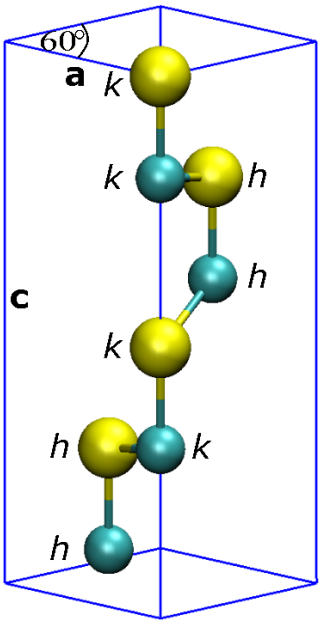

Fig. 4 Cell expansion (111, hexagonal unit cell) of 4H-SiC indicating cell parameters (*a*, *c*) and hexagonal (*h*), cubic (*k*) atom positions; carbon = teal, silicon = yellow

Table 1 Cell expansions and k-point meshes used in the calculations

Cell	221	331	341	441	551	661	771	881
Mesh	442	332	322	222	222	222	222	222
Cell	991	222	332	442	552	662	772	. . .
Mesh	222	441	331	221	221	221	221	. . .

We investigated properties of the *hh* divacancy defect in 4H-SiC (Figs. 2 and 4). We compared full defect relaxation including lattice and ionic position optimization with ionic position optimization only; the latter is termed partial. Defect formation energies were calculated as

$$E_f = E_d - E_b + \mu_C + \mu_{Si} + \Delta H_f + q(E_{Fermi} + VBM) + E^c, \quad (1)$$

where E_d is the defect energy, E_b the bulk energy, μ_C the chemical potential of carbon, μ_{Si} the chemical potential of silicon, q the charge state of the defect, E_{Fermi} the Fermi energy, and *VBM* the valence band maximum of the bulk. The enthalpy of formation of SiC, ΔH_f, was added assuming a carbon-rich environment. The energy term E^C corrects for interactions of periodically repeated charged defects and the interaction of the defect with the uniform background charge that is introduced by QE in calculations of charged systems. We used the code sxdefectalign[40,41] to compute E^C. To obtain E_d and E_b consistently in Eq. 1, the bulk lattice and ionic positions were optimized using the same cell expansion and k-point mesh as for the defect calculation.

For the 552 cell expansion we computed 2 spin states per charge state. The most-stable spin states for the neutral, –1, +1, –2, and +2 *hh* defects are the triplet, doublet (–1, +1), and singlet (–2, +2) states, respectively, confirming the results in Iwata et al.[27] For all other cell expansions and charge states, we computed the spin states that were determined to be lowest using the 552-cell expansion.

We used the constrained DFT formalism to compute excitation energies for the neutral triplet state of the *hh* divacancy defect. Since constrained DFT is implemented in QE for Gamma-point calculations only, all excitation energies are given relative to the Gamma-point ground state energy for which the geometry was obtained employing the k-point mesh as previously outlined. The local symmetry of the *hh* defect is C_{3v}. The absorption energies were calculated using the ground state geometries and by promoting an electron within the minority spin block from the defect a state (highest occupied state), to the defect e state (lowest unoccupied state) with occupation 0.5 per degenerate single electron wave function. The local defect a and e states of the ground state are visualized in Fig. 5. When only one of the e states was occupied, the vertically excited state did not converge. When either full or partial relaxation of the excited state was allowed, we obtained excited states with 0.5/0.5 and 1/0 occupation of the e states. Using 0.5/0.5 occupancy of the e state maintained degeneracy in the excited state while 1/0 occupation caused a splitting of the e states in the excited state. The 1/0 adiabatic excited state was calculated to be lower in energy than the excited state with partial occupation. ZPLs were calculated as the difference between the structurally relaxed excited and the ground state. The emission energy is the energy difference between relaxed excited state and the ground state at excited state geometry.

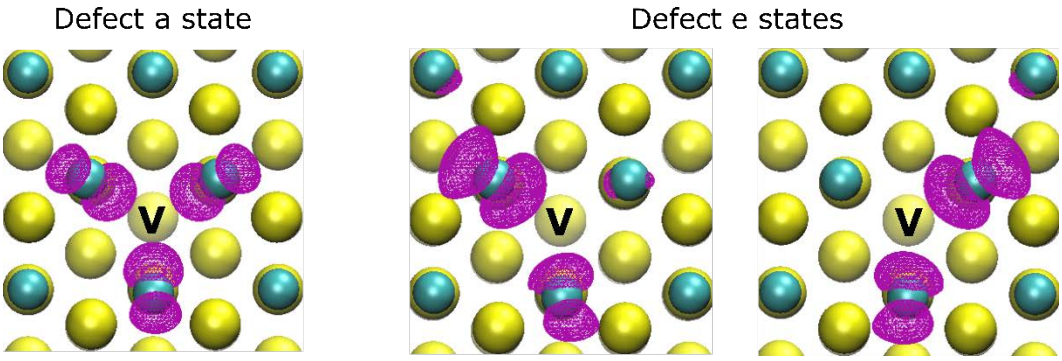

Fig. 5 Defect states of the neutral triplet *hh* divacancy in 4H-SiC using a 552-cell expansion; v = divacancy, carbon = teal, silicon = yellow

3. Results and Discussion

In the following we discuss properties of the *hh* divacancy in 4H-SiC that are relevant to the study of the defect as a candidate qubit. We compare the convergence of these properties with respect to the computational cell size within the DFT framework with and without the inclusion of dispersion effects and for full and partial structural relaxation of the defect.

3.1 Defect Formation Energy

The charge state of the divacancy in 4H-SiC that has been shown to function as a qubit is the neutral charge state. The concentration of that defect in 4H-SiC can be related to the defect formation energy, which we investigate in the following. Figure 6 shows the formation energy of the neutral triplet divacancy defect in 4H-SiC as a function of the computational cell parameter *a* (see Fig. 4). Initially, we used increasing cell expansions in *a*, while the cell expansion in *c* was kept at one. We observed that defect formation energy differences between full and partial structural relaxation were below 0.01 eV for cell expansions larger than 221 (a = 6 Å), indicating that the lattice parameters of the bulk can be used for defect calculations. Although the values of the defect formation energy differ by about 0.5 eV, we find the same convergence behavior with respect to cell size for calculations with and without dispersion corrections. For the 551-cell expansion (a = 15 Å) and larger, we expected an error in the defect formation energy due to finite cell size along *a* below 0.05 eV. Figure 7 depicts the formation energy of the neutral defect as a function of the cell parameter *a* using a cell expansion in *c* of twice the lattice parameter. Again, partial relaxation is sufficient for defect formation energy calculations. Although the defect formation energy is not a monotonic function of *a* when dispersion is not included, we expected an error below 0.05 eV due to finite size effects along *a* for the defect formation energy when a 552-cell expansion (a = 15 Å) or larger is used with and without dispersion corrections.

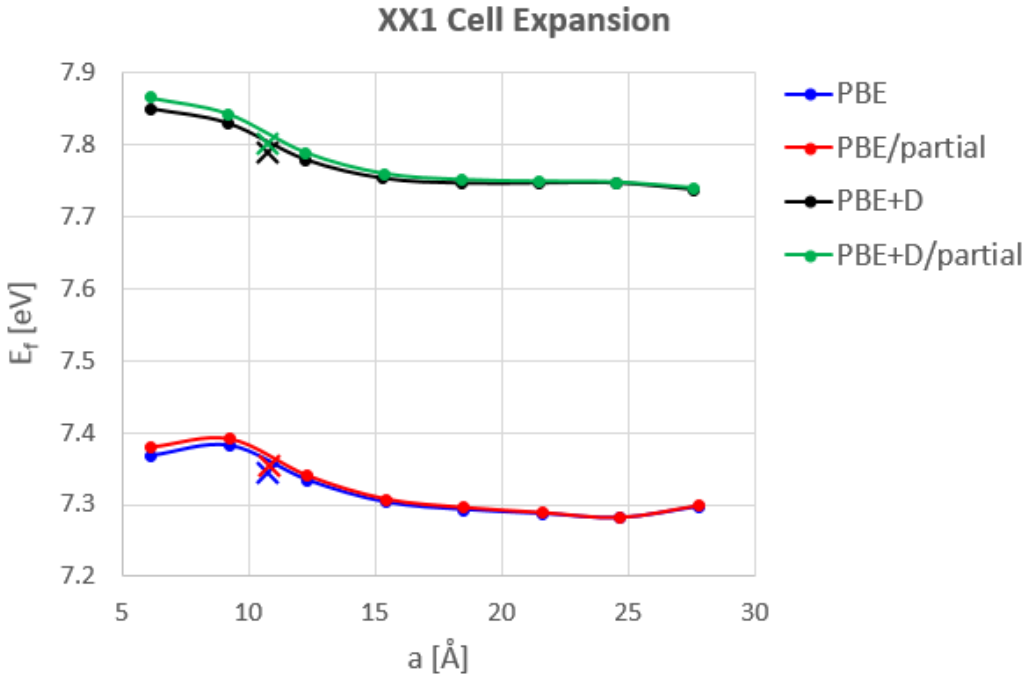

Fig. 6 Defect formation energy (E_f) in electronvolts (eV) for the *hh* divacancy defect in 4H-SiC as a function of the cell parameter *a* in Å while *c* is kept at unit cell value, PBE with and without dispersion (D), and full and partial relaxation. Data points marked x are obtained with the 341-cell expansion, and values for *a* are averaged.

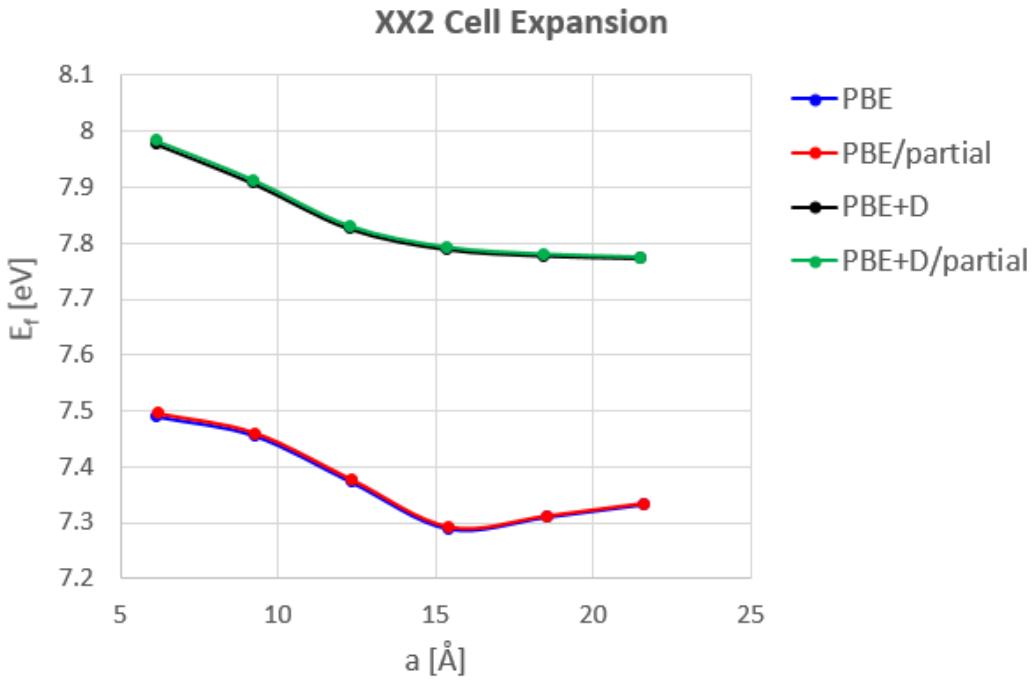

Fig. 7 Defect E_f in eV for the *hh* divacancy defect in 4H-SiC as a function of the cell parameter *a* in Å while *c* is kept at twice the unit cell value, PBE with and without D, and full and partial relaxation

To compare defect formation energies for cell expansions along all directions, we plotted the defect formation energies obtained with the PBE functional without dispersion correction, and with full relaxation, as a function of *a* for expansions of 1 and 2 along *c* in Fig. 8. The defect formation energy tends to decrease with increasing *a* (with some irregularities likely due to error sources other than finite size effects), while it typically increases with increasing *c* (see Fig. 4). However, when a 551 expansion (*a* = 15 Å) or larger is employed in *a*, a combined error due to finite size effects in *a* as well as in *c* of below 0.05 eV is estimated. To ensure that our conclusion is not affected by using too small of an expansion along *c*, we calculated the defect formation energy for a 443 expansion (*a* = 12 Å), which differs from the defect formation energy for the 442 expansion by less than 0.01 eV (Fig. 8). We have also included the defect formation energy for the 341 expansion (marked with x in Figs. 6 and 8) since it has been reported to yield ZPLs to within 0.1-eV accuracy[34] with respect to all computational error sources. According to our results, the error in the defect formation energy due to finite size effects for the 341 expansion is on the order of 0.1 eV. Overall, we recommend a 551 expansion of the computational cell for the calculation of the formation energy of the neutral defect yielding an error below 0.05 eV due to finite size effects.

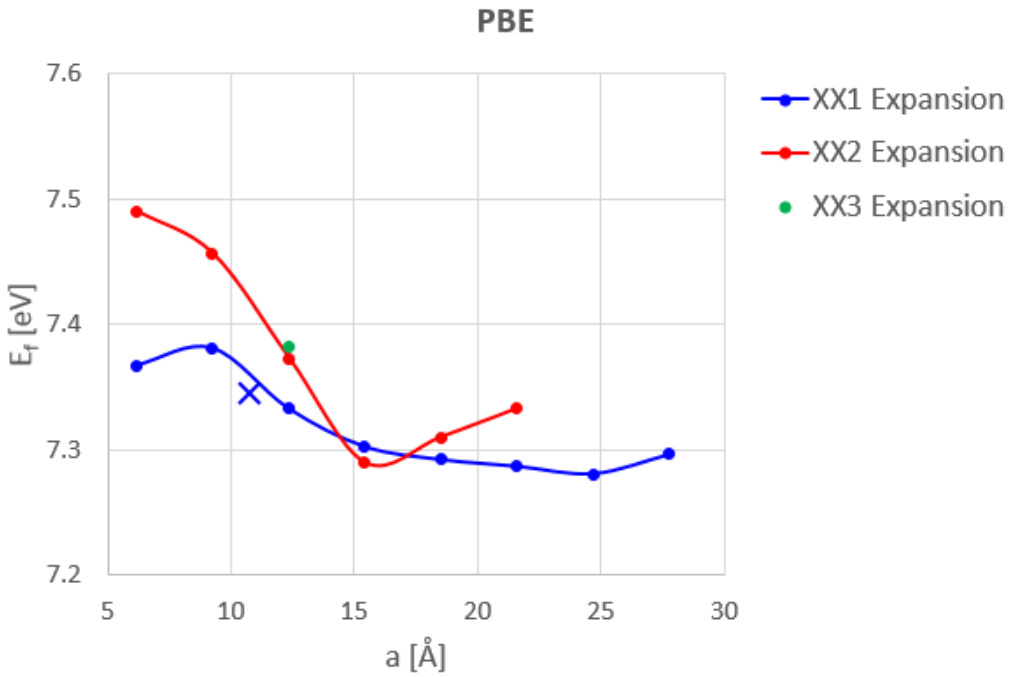

Fig. 8 Defect E_f in eV for the *hh* divacancy defect in 4H-SiC as a function of the cell parameter *a* in Å, PBE without D, and full relaxation. Data point marked x is obtained with the 341-cell expansion, and the value for *a* is averaged.

3.2 Defect Level Position

Bandgaps and defect level positions have to fulfill certain criteria for a defect to be viable as a qubit.[10] Also, methods that go beyond DFT (GW/ Bethe-Salpeter) often use DFT wave functions and single particle energies to improve upon. In this section we analyze the defect level position of the highest occupied defect level (a state in Fig. 5) relative to the valence band maximum of the bulk ($\Delta\varepsilon$). We do not attempt convergence testing for band gaps or unoccupied single particle energies since the latter have only little meaning within the DFT framework.

Figure 9 shows $\Delta\varepsilon$ as a function of the cell parameter *a* when maintaining *c* at the unit cell value. It appears that the defect level position is not converged with respect to computational cell size in *a*. Notice, however, that the difference in $\Delta\varepsilon$ over the entire range of *a* does not exceed 0.07 eV. Trends for PBE with and without dispersion as well as full and partial relaxation are very similar. In contrast to defect formation energies, where the inclusion of dispersion has a much larger effect than the relaxation scheme, we find that the effect of dispersion on the defect level is of similar magnitude to the relaxation of the lattice parameter in the defect calculations: neither exceeds 0.04 eV. In Fig. 10, we plot $\Delta\varepsilon$ as a function of the cell parameter *a* for a cell expansion of 2 along *c*. Again, trends for PBE with and without dispersion, as well as full and partial relaxation, are similar. $\Delta\varepsilon$ reaches convergence with *a*, yielding a residual error of about 0.02 eV for a 552-cell expansion (a = 15 Å). Notice that the difference in $\Delta\varepsilon$ (0.5 eV) over the range of *a* is very large compared with the data shown in Fig. 9. Also, the effect of dispersion or lattice parameter relaxation in the defect calculations does not exceed 0.02 eV in $\Delta\varepsilon$.

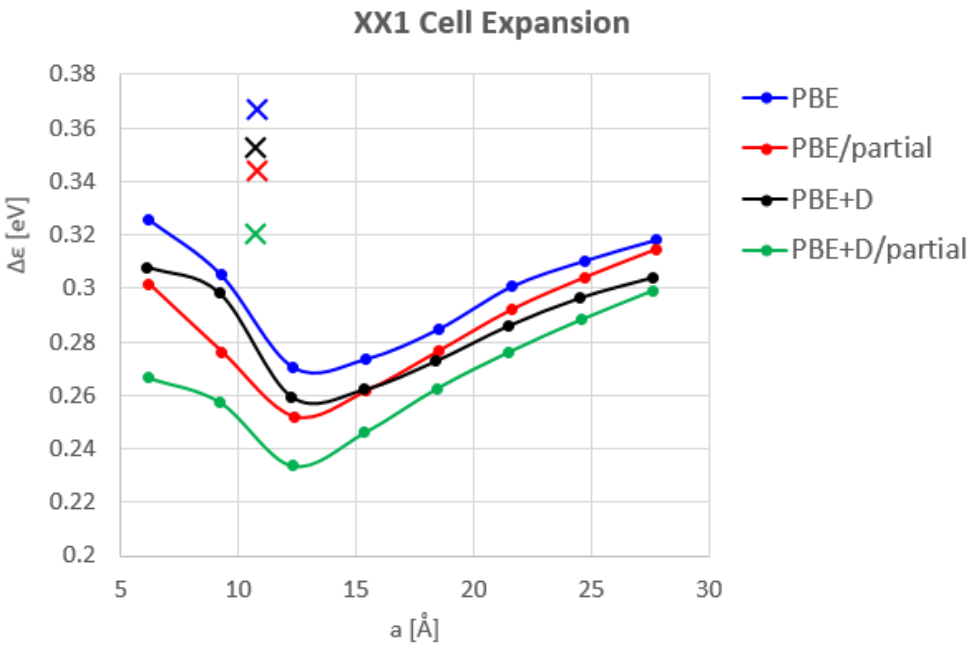

Fig. 9 Highest occupied defect level relative to bulk valence band maximum (Δε) in eV for the *hh* divacancy defect in 4H-SiC as a function of the cell parameter *a* in Å while *c* is kept at unit cell value, PBE with and without D, and full and partial relaxation. Data points marked x are obtained with the 341-cell expansion, and values for *a* are averaged.

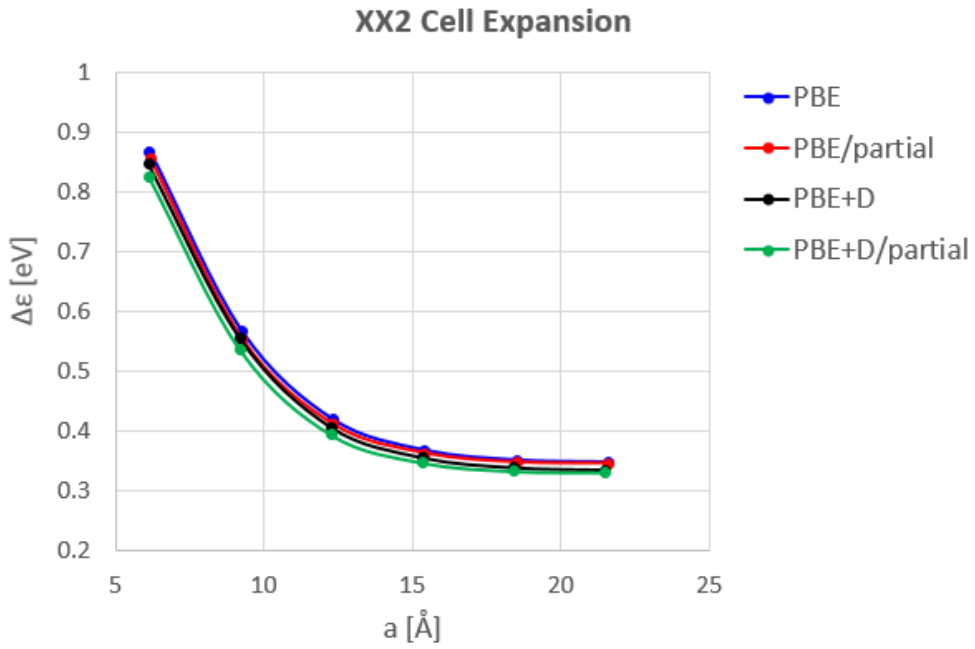

Fig. 10 Highest occupied defect level relative to Δε in eV for the *hh* divacancy defect in 4H-SiC as a function of the cell parameter *a* in Å while *c* is kept at twice the unit cell value, PBE with and without D, and full and partial relaxation

In Fig. 11 we compare the dependence of Δε on the cell parameter *a* for an expansion of 1 (XX1) and 2 (XX2) along *c* using PBE without dispersion and full relaxation. We also include the value of Δε for a 443 expansion (*a* = 12 Å), which is 0.05 eV larger than Δε for the 442 expansion. Although this indicates that testing should be continued to include a data series with an expansion of 3 along *c*, these calculations are too resource-intensive for this work. From Fig. 11, we determine that for the calculation of defect levels, a cell expansion of no less than 552 should be used. The error due to finite size effects is difficult to estimate but is expected to be smaller than 0.05 eV (difference in Δε between 442 and 443 expansion). For a 341-cell expansion, we observe a fortuitous error cancellation between size effects along *a* and *c*.

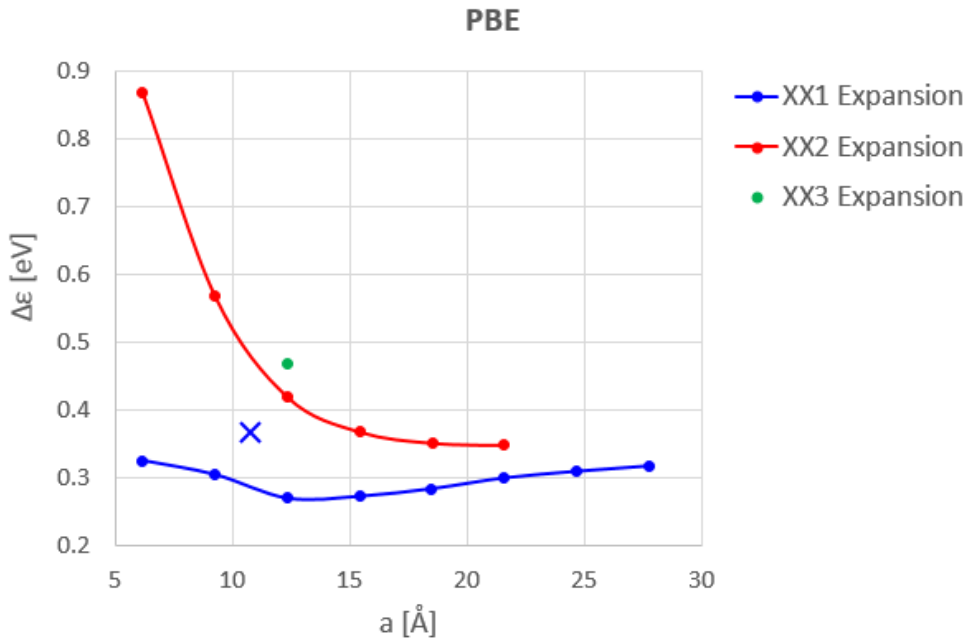

Fig. 11 Highest occupied defect level relative to Δε in eV for the *hh* divacancy defect in 4H-SiC as a function of the cell parameter *a* in Å, PBE without D, and full relaxation. Data point marked x is obtained with the 341-cell expansion, and the value for *a* is averaged.

3.3 Charge Transition Levels

The calculation of the formation energies for possible defect charge states, as a function of the Fermi level (which may be varied experimentally through doping), determines the most likely charge state. In 4H-SiC, an optical switching between divacancy charge states has been observed.[42,43] The hypothesized mechanisms involve a +1 charge state[42] and a –1 charge state.[43] Determining computationally if, and for which, Fermi levels a charge transition between the neutral and the +1 or –1 charge state occurs may strengthen either hypothesis. The calculation of formation energies for charged defects converges very slowly with cell size due to

the long-ranged Coulomb interactions between periodic images. This is compensated for by the inclusion of a correction term as discussed in Section 2.

The *hh* divacancy defect formation energy of the neutral, +1, –1, +2, and –2 charge states in their most stable spin states (see Section 2) as a function of the E_{Fermi} for a 551-cell expansion calculated with PBE without dispersion and full relaxation is plotted in Fig. 12. The E_{Fermi} ranges from 0 to the experimental band gap of 3.23 eV,[14] and the dotted line in the figure indicates the location of the PBE band edge. The black line traces the most stable charge state (lowest defect formation energy) as a function of the E_{Fermi}. The neutral divacancy, which is the defect state observed in photoluminescence spectra,[21] is most stable for an E_{Fermi} between 0.3 and 1.4 eV. At lower and higher E_{Fermi}'s, we observe a stability window of 0.3 eV for the +1 and –1 charge states. Although this finding does not disqualify the charge state conversion mechanism involving neither the +1 nor the –1 charge state, it suggests control of the mechanism through doping, shifting the probability of charge state creation toward the +1 or –1 charge state. Our results are similar to previously published PBE data[27] for transition levels and defect formation energies. Note, however, the sensitivity of the transition levels to the functional choice. The Heyd-Scuseria-Ernzerhof (HSE) functional yields a defect formation energy for the neutral divacancy that is 0.8 eV higher than that computed with the PBE functional[27] resulting in shifts in the transition levels by 0.5 eV.[27,34]

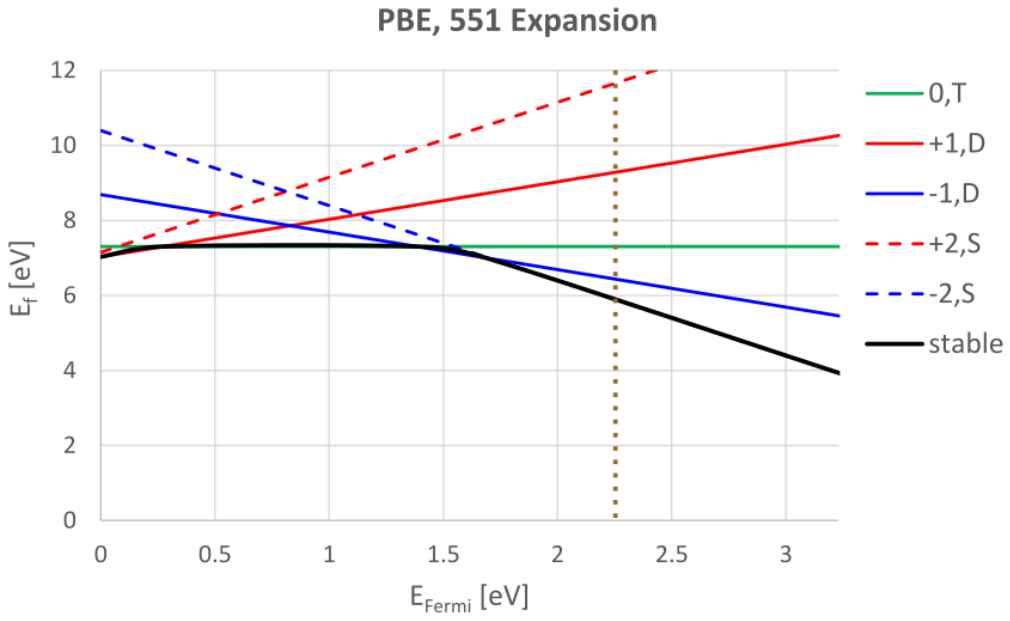

Fig. 12 Defect E_f in eV for the *hh* divacancy defect in 4H-SiC as a function of the E_{Fermi} in eV relative to the valence band maximum sweeping from 0 eV to the experimental band gap for the neutral triplet (0, T), +1 doublet (+1, D), –1 doublet (–1, D), +2 singlet (+2, S), –2 singlet (–2, S), and most stable states. PBE band gap indicated by vertical dotted line, 551-cell expansion, PBE without D, and full relaxation.

Since we determined that a cell expansion of at least 551 is required to compute defect formation energies of the neutral *hh* divacancy, we investigated the dependence of the transition levels on computational cell size starting with a 551 expansion and extending to 552-, 661-, 662-, 771-, and 772-cell expansions. We added the 341 expansion because of its use in the literature.[34] The corresponding transition levels for the different cell expansions computed with and without dispersion, as well as full and partial relaxation, are given in the Appendix (Figs. A-1 to A-7). Although the defect formation energy difference between the neutral divacancy computed with and without dispersion (0.5 eV) is nearly as large as the difference computed with PBE and HSE (0.8 eV),[27] the effect of dispersion on the transition levels is less than the effect of exact exchange interactions, indicating a more consistent impact of dispersion on the different charge states. Dispersion has a larger influence on the +1/0 transition level (0.1 eV) than it has on the –1/0 and –1/–2 transition levels (0.02 eV). Lattice relaxation in the defect calculations affects the transition levels for the 341 expansion more than for larger cells. For 551 and larger cell expansions, the effect of lattice relaxation is below 0.1 eV for transition levels involving negative charge states but is higher for the +1/0 transition level with up to 0.18 eV.

In Fig. 13, we plot the E_{Fermi} at which charge transition occurs as a function of the cell parameter *a* calculated without dispersion and full relaxation. A series of lattice expansions along *a*, for an expansion of 1 (XX1) and 2 (XX2) along *c*, are compared. Using a 341 expansion (a = 11 Å), we expect an error of about 0.2 eV in the transition levels due to finite size effects. We do not observe systematic convergence behavior with cell size for the +1/0 transition. The transition levels involving negative charge states appear converged with respect to cell size using a 551-cell expansion (a = 15 Å) with a residual error of 0.01 eV. The same conclusion can be drawn from a plot of the transition levels calculated with inclusion of dispersion interactions and full relaxation in Fig. A-8 of the Appendix. Note that the 551 expansion was used in the preceding discussion and in Fig. 12. While we estimate an error of 0.01 eV in transition levels due to finite size effects for a 551-cell expansion, nonsystematic errors of 0.2 eV evidently occur in the calculation of formation energies for charged defects.

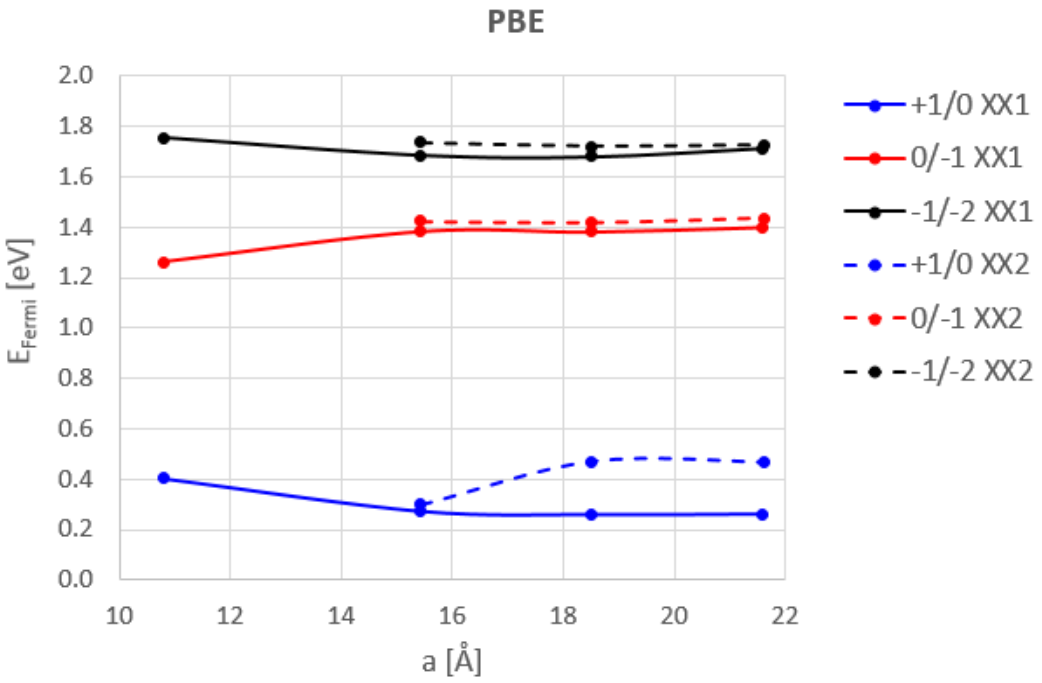

Fig. 13 E_{Fermi} in eV for the *hh* divacancy defect in 4H-SiC at which transition between +1 and neutral (+1/0), neutral and –1 (0/–1), –1 and –2 (–1/–2) charge states occurs as a function of the cell parameter *a* in Å, PBE without D, and full relaxation

3.4 Zero Phonon Line

The ZPL is the energy difference between the ^{3}A state and the structurally relaxed excited ^{3}E state, as displayed in Fig. 3. This transition is vital for the optical initialization and read-out of the qubit states and is measured in photoluminescence spectra.[21] In this final section, we analyze the convergence properties of the ZPL for the *hh* divacancy with respect to computational cell size.

The absorption, zero phonon, and emission lines for the same cell expansions as those used for transition levels in Section 3.3 calculated, with and without dispersion, as well as full and partial relaxation, are given in Figs. A-9 to A-15 of the Appendix. The inclusion of dispersion consistently increases all excitation energies by 0.06 to 0.08 eV for all cell expansions considered. While the error due to the neglect of lattice relaxation in the defect states for the 341 expansion reaches up to 0.05 eV, it is 0.01 eV or below for the 551 expansion and larger.

Figure 14 contains excitation energies as a function of the cell parameter *a* for an expansion of 1 (XX1) and 2 (XX2) along *c* calculated without dispersion and full relaxation. While the difference in excitation energies between the XX1 and XX2 expansions is small, a maximum deviation of 0.03 eV for the ZPL using a 77X expansion, the excitation energies continue to decrease for increasing *a*. To reduce

the error resulting from finite size effects to a threshold of 0.1 eV for ZPLs, we estimate that a 661 expansion (a = 19 Å) is required. The same conclusion can be drawn from the plot of the excitation energies as a function of a calculated with dispersion and full relaxation given in Fig. A-16 of the Appendix. Note that QE only allows for Gamma point calculations when employing constrained DFT, which may influence some of the observed convergence behavior. Table 2 compares excitation energies calculated previously with HSE and a 96-atom supercell (341 expansion),[34] the ZPL computed with HSE and a 432-atom supercell,[32] the experimental ZPL for the *hh* divacancy,[21] and our PBE results for the 661-cell expansion (286-atom supercell) with and without dispersion. It is unclear what k-point mesh was used in the previous computations. Although our value for the ZPL calculated with PBE including dispersion interactions and full relaxation deviates from the experimental ZPL by only 0.05 eV, the agreement is most likely fortuitous since the error due to cell size expansion is of the same order, and errors due to the neglect of k-point sampling beyond the Gamma point for excitation energies, functional choice, and pseudopotential are unknown.

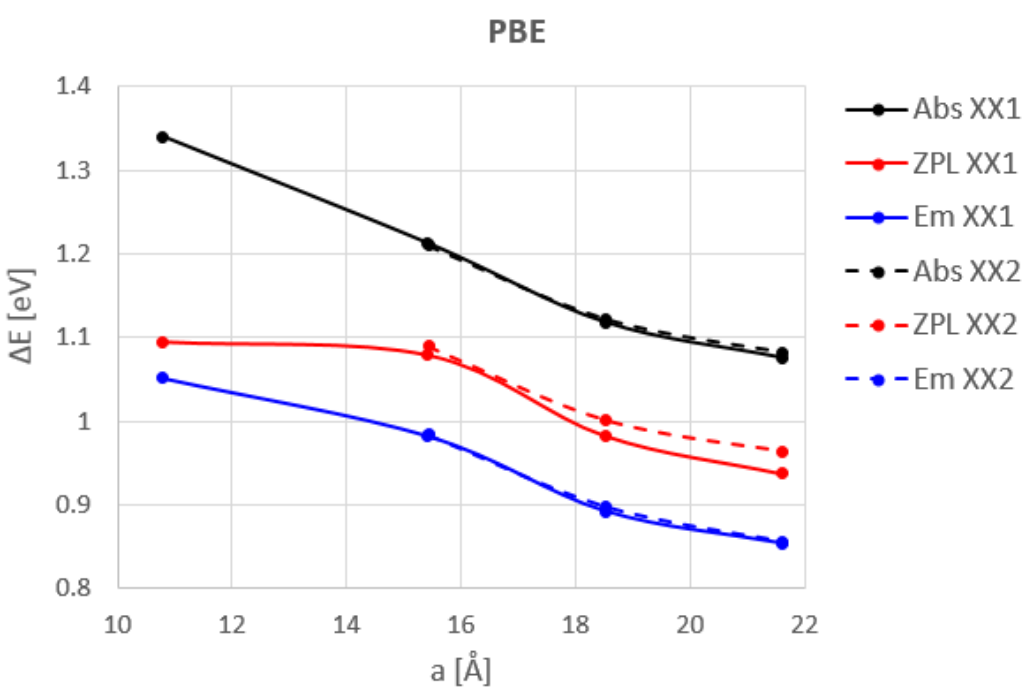

Fig. 14 Absorption (Abs), ZPL, and emission (Em) lines in eV for the *hh* divacancy defect in 4H-SiC as a function of the cell parameter *a* in Å, PBE without D, and full relaxation

Table 2 Abs, ZPL, and Em lines for the *hh* divacancy defect in 4H-SiC in eV comparing calculated and experimental literature values with PBE results with and without D using full relaxation and a 661-cell expansion

Line	Ref. [34]	Ref. [32]	PBE	PBE+D	Exp. [21]
Abs	1.18	. . .	1.12	1.19	. . .
ZPL	1.13	1.06	0.98	1.05	1.095
Em	1.09	. . .	0.89	0.95	. . .

4. Conclusions

We investigated ground and excited state properties of the *hh* divacancy defect in 4H-SiC. Its neutral charge state can function as a qubit that is individually addressable in the near IR.[20] Other charge states may also play a role in quantum information storage and have been reported to be intermediate states in optical experiments.[42,43] We focused on the calculation of properties that are relevant to the defect functioning as a qubit.

We computed defect formation energies of the neutral and charged *hh* divacancy with corresponding charge transition levels, the position of the highest occupied, localized defect state within the band gap, and excitation energies for the ^{3}A to ^{3}E transition (Abs, ZPL, and Em), which is essential for optical initialization and read-out of the qubit. We used the PBE functional but believe that the results are transferable to other DFT functionals. In particular, we studied convergence behavior with respect to computational cell size and compared results with and without the inclusion of dispersion interactions. In addition, we contrasted results obtained with full defect relaxation including lattice and ionic relaxation with values calculated with partial relaxation carrying out ionic defect relaxation only.

We found that the error due to the omission of lattice relaxation in the defect calculations tends to be small but should not be neglected for the determination of defect level positions and, especially, for the computation of charge transition levels, which requires the calculation of formation energies of charged defects. While dispersion interactions influence property values, trends in cell size dependence are similar in calculations with and without the inclusion of dispersion. For the computation of the formation energy of the neutral divacancy defect, we recommend a 551-cell expansion, yielding an error due to finite cell size below 0.05 eV. The same cell expansion appears converged with respect to computational cell size for the calculation of charge transition levels with an approximate error of 0.01 eV. However, we observe unsystematic errors in the charge transition levels of 0.2 eV. The calculation of the position of the local defect states relative to the bulk valence band maximum requires a 552-cell expansion to reduce errors

resulting from finite cell size to below 0.05 eV. Finally, we recommend a 661 expansion for the calculation of the ZPL with an estimation of the error due to finite cell size of below 0.1 eV. The analysis of the convergence properties of the ZPL is complicated by the fact that constrained DFT, as implemented in QE, can only be performed at Gamma point.

Although we obtained agreement between the experimental ZPL and the ZPL calculated with PBE including dispersion and a 661-cell expansion to within 0.05 eV, our estimated error due to finite cell size alone is 0.1 eV, and errors due to functional choice, k-point sampling, and pseudopotential are unknown. We advocate caution when deriving computational accuracy from the comparison of computed ZPLs and experimental results without proper error analysis with respect to computational parameters.

5. References

1. Shi X, Wei LF, Oh CH. Quantum computation with surface-state electrons by rapid population passages. Science China-Physics Mechanics and Astronomy. 2014;57(9):1718–1724.

2. Platzman PM, Dykman MI. Quantum computing with electrons floating on liquid helium. Science. 1999;284(5422):1967–1969.

3. Cory DG, Laflamme R, Knill E, Viola L, Havel TF, Boulant N, Boutis G, Fortunato E, Lloyd S, Martinez R, et al. NMR-based quantum information processing: achievements and prospects. Fortschritte Der Physik – Progress of Physics. 2000;48(9–11):875–907.

4. Wang L, Tu T, Gong B, Guo GC. Decoherence-protected spin-photon quantum gates in a hybrid semiconductor-superconductor circuit. Physical Review A. 2015;92(6).

5. Hassler F, Catelani G, Bluhm H. Exchange interaction of two spin qubits mediated by a superconductor. Physical Review B. 2015;92(23).

6. Walther A, Rippe L, Yan Y, Karlsson J, Serrano D, Nilsson AN, Bengtsson S, Kroll S. High-fidelity readout scheme for rare-earth solid-state quantum computing. Physical Review A. 2015;92(2).

7. Serrano D, Yan Y, Karlsson J, Rippe L, Walther A, Kroll S, Ferrier A, Goldner P. Impact of the ion-ion energy transfer on quantum computing schemes in rare-earth doped solids. Journal of Luminescence. 2014;151:93–99.

8. Debnath S, Linke NM, Figgatt C, Landsman KA, Wright K, Monroe C. Demonstration of a small programmable quantum computer with atomic qubits. Nature. 2016;536(7614):63.

9. Gordon L, Weber JR, Varley JB, Janotti A, Awschalom DD, van de Walle CG. Quantum computing with defects. Mrs Bulletin. 2013;38(10):802–807.

10. Weber JR, Koehl WF, Varley JB, Janotti A, Buckley BB, Van de Walle CG, Awschalom DD. Quantum computing with defects. Proceedings of the National Academy of Sciences of the United States of America. 2010;107(19):8513–8518.

11. Childress L, Dutt MVG, Taylor JM, Zibrov AS, Jelezko F, Wrachtrup J, Hemmer PR, Lukin MD. Coherent dynamics of coupled electron and nuclear spin qubits in diamond. Science. 2006;314(5797):281–285.

12. Neumann P, Mizuochi N, Rempp F, Hemmer P, Watanabe H, Yamasaki S, Jacques V, Gaebel T, Jelezko F, Wrachtrup J. Multipartite entanglement among single spins in diamond. Science. 2008;320(5881):1326–1329.

13. Dutt MVG, Childress L, Jiang L, Togan E, Maze J, Jelezko F, Zibrov AS, Hemmer PR, Lukin MD. Quantum register based on individual electronic and nuclear spin qubits in diamond. Science. 2007;316(5829):1312–1316.

14. Goldberg Y, Levinshtein ME, Rumyantsev SL. In: Levinshtein ME, Rumyantsev SL, Shur MS, editors. Properties of advanced semiconductor materials GaN, AlN, SiC, BN, SiC, SiGe. New York (NY): John Wiley & Sons; 2001. p. 93–148.

15. Persson C, Lindefelt U. Relativistic band structure calculation of cubic and hexagonal SiC polytypes. Journal of Applied Physics. 1997;82(11):5496–5508.

16. Isoya J, Umeda T, Mizuochi N, Son NT, Janzen E, Ohshima T. EPR identification of intrinsic defects in SiC. Physica Status Solidi B-Basic Solid State Physics. 2008;245(7):1298–1314.

17. von Bardeleben HJ, Cantin JL, Csore A, Gali A, Rauls E, Gerstmann U. NV centers in 3C, 4H, and 6H silicon carbide: a variable platform for solid-state qubits and nanosensors. Physical Review B. 2016;94(12).

18. Umeda T, Ishoya J, Ohshima T, Morishita N, Itoh H, Gali A. Identification of positively charged carbon antisite-vacancy pairs in 4H-SiC. Physical Review B. 2007;75(24).

19. Weber JR, Koehl WF, Varley JB, Janotti A, Buckley BB, van de Walle CG, Awschalom DD. Defects in SiC for quantum computing. Journal of Applied Physics. 2011;109(10).

20. Christle DJ, Falk AL, Andrich P, Klimov PV, Ul Hassan J, Son NT, Janzen E, Ohshima T, Awschalom DD. Isolated electron spins in silicon carbide with millisecond coherence times. Nature Materials. 2015;14(2):160–163.

21. Koehl WF, Buckley BB, Heremans FJ, Calusine G, Awschalom DD. Room temperature coherent control of defect spin qubits in silicon carbide. Nature. 2011;479(7371):84–U108.

22. Carlsson P, Son NT, Gali A, Isoya J, Morishita N, Ohshima T, Magnusson B, Janzen E. EPR and ab initio calculation study on the EI4 center in 4H- and 6H-SiC. Physical Review B. 2010;82(23).

23. Umeda T, Ishitsuka Y, Isoya J, Son NT, Janzen E, Morishita N, Ohshima T, Itoh H, Gali A. EPR and theoretical studies of negatively charged carbon vacancy in 4H-SiC. Physical Review B. 2005;71(19).

24. Bockstedte M, Heid M, Pankratov O. Signature of intrinsic defects in SiC: ab initio calculations of hyperfine tensors. Physical Review B. 2003;67(19).

25. Son NT, Carlsson P, Ul Hassan J, Janzen E, Umeda T, Isoya J, Gali A, Bockstedte M, Morishita N, Ohshima T, Itoh H. Divacancy in 4H-SiC. Physical Review Letters. 2006;96(5).

26. Trinh XT, Szasz K, Hornos T, Kawahara K, Suda J, Kimoto T, Gali A, Janzen E, Son NT. Negative-U carbon vacancy in 4H-SiC: assessment of charge correction schemes and identification of the negative carbon vacancy at the quasicubic site. Physical Review B. 2013;88(23).

27. Iwata JI, Shinei C, Oshiyama A. Density-functional study of atomic and electronic structures of multivacancies in silicon carbide. Physical Review B. 2016;93(12).

28. Torpo L, Staab TEM, Nieminen RM. Divacancy in 3C- and 4H-SiC: an extremely stable defect. Physical Review B. 2002;65(8).

29. Torpo L, Marlo M, Staab TEM, Nieminen RM. Comprehensive ab initio study of properties of monovacancies and antisites in 4H-SiC. Journal of Physics-Condensed Matter. 2001;13(28):6203–6231.

30. Zywietz A, Furthmuller J, Bechstedt F. Vacancies in SiC: influence of Jahn-Teller distortions, spin effects, and crystal structure. Physical Review B. 1999;59(23):15166–15180.

31. Oda T, Zhang YW, Weber WJ. Study of intrinsic defects in 3C-SiC using first-principles calculation with a hybrid functional. Journal of Chemical Physics. 2013;139(12).

32. Zargaleh SA, Eble B, Hameau S, Cantin JL, Legrand L, Bernard M, Margaillan F, Lauret JS, Roch JF, von Bardeleben HJ, et al. Evidence for near-infrared photoluminescence of nitrogen vacancy centers in 4H-SiC. Physical Review B. 2016;94(6).

33. Csore A, von Bardeleben HJ, Cantin JL, Gali A. Characterization and formation of NV centers in 3C, 4H, and 6H SiC: an ab initio study. Physical Review B. 2017;96(8).

34. Gordon L, Janotti A, van de Walle CG. Defects as qubits in 3C- and 4H-SiC. Physical Review B. 2015;92(4).

35. Gali A. Time-dependent density functional study on the excitation spectrum of point defects in semiconductors. Physica Status Solidi B-Basic Solid State Physics. 2011;248(6):1337–1346.

36. Giannozzi P, Baroni S, Bonini N, Calandra M, Car R, Cavazzoni C, Ceresoli D, Chiarotti GL, Cococcioni M, Dabo I, et al. QUANTUM ESPRESSO: a modular and open-source software project for quantum simulations of materials. Journal of Physics-Condensed Matter. 2009;21(39).

37. Perdew JP, Burke K, Ernzerhof M. Generalized gradient approximation made simple. Physical Review Letters. 1996;77(18):3865–3868.

38. Grimme S. Semiempirical GGA-type density functional constructed with a long-range dispersion correction. Journal of Computational Chemistry. 2006;27(15):1787–1799.

39. Barone V, Casarin M, Forrer D, Pavone M, Sambi M, Vittadini A. Role and effective treatment of dispersive forces in materials: polyethylene and graphite crystals as test cases. Journal of Computational Chemistry. 2009;30(6):934–939.

40. Freysoldt C, Neugebauer J, van de Walle CG. Fully ab initio finite-size corrections for charged-defect supercell calculations. Physical Review Letters. 2009;102(1).

41. Freysoldt C, Neugebauer J, van de Walle CG. Electrostatic interactions between charged defects in supercells. Physica Status Solidi B-Basic Solid State Physics. 2011;248(5):1067–1076.

42. Golter DA, Lai CW. Optical switching of defect charge states in 4H-SiC. Scientific Reports. 2017;7.

43. Wolfowicz G, Anderson CP, Yeats A, Whiteley SJ, Niklas J, Poluektov O, Heremans FJ, Awschalom DD. Optical charge state control of spin defects in 4H-SiC. Nature Communications. 2017;8.

Appendix. Supplementary Charge Transition Levels and Zero Phonon Line (ZPL)

A.1 Charge Transition Levels

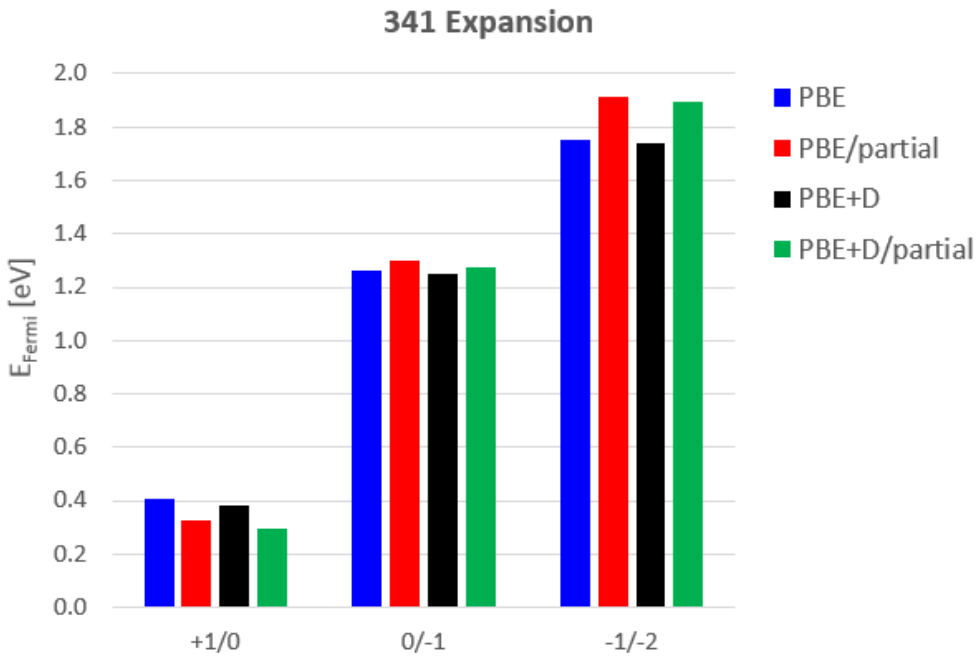

Fig. A-1 Fermi energy (E_{Fermi}) in eV for the *hh* divacancy defect in 4H-SiC at which transition between +1 and neutral (+1/0), neutral and –1 (0/–1), –1 and –2 (–1/–2) charge states occurs for the 341-cell expansion, Perdew-Burke-Ernzerhof (PBE) with and without dispersion (D), and full and partial relaxation

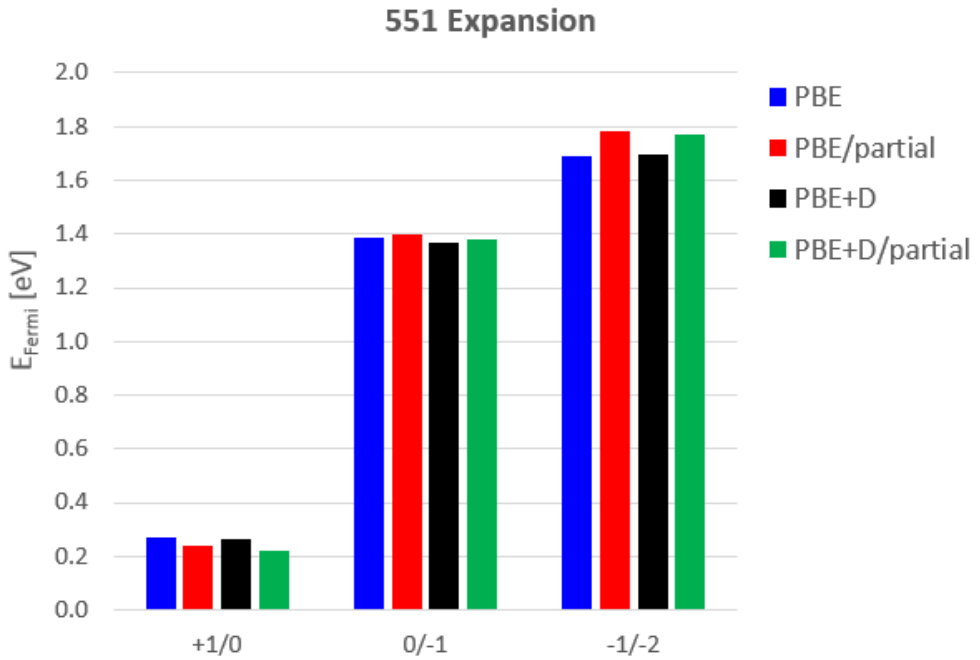

Fig. A-2 E_{Fermi} in eV for the *hh* divacancy defect in 4H-SiC at which transition between +1 and neutral (+1/0), neutral and –1 (0/–1), –1 and –2 (–1/–2) charge states occurs for the 551-cell expansion, PBE with and without D, and full and partial relaxation

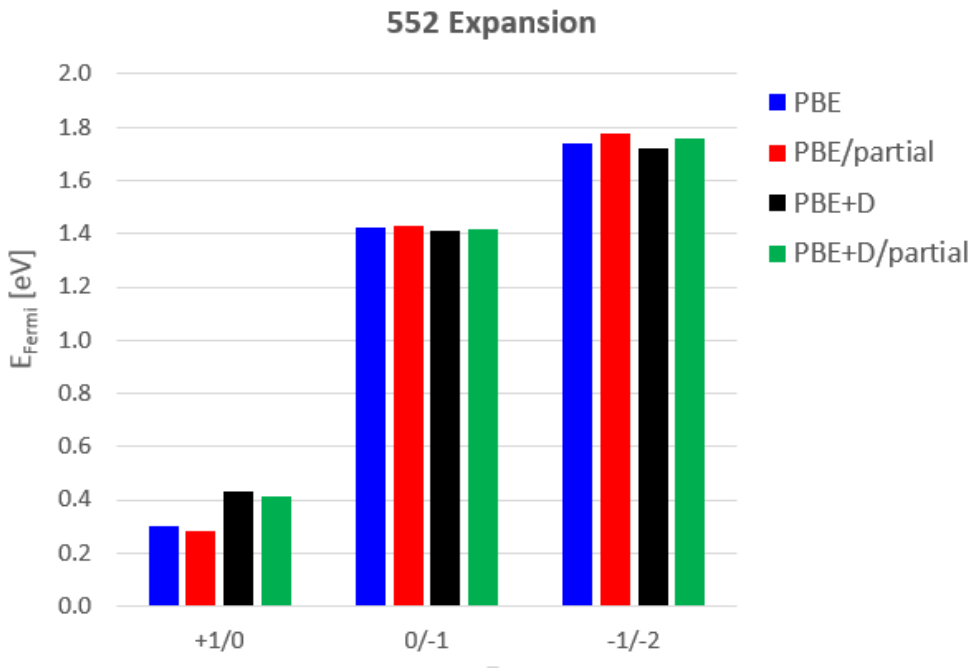

Fig. A-3 E_{Fermi} in eV for the *hh* divacancy defect in 4H-SiC at which transition between +1 and neutral (+1/0), neutral and –1 (0/–1), –1 and –2 (–1/–2) charge states occurs for the 552-cell expansion, PBE with and without D, and full and partial relaxation

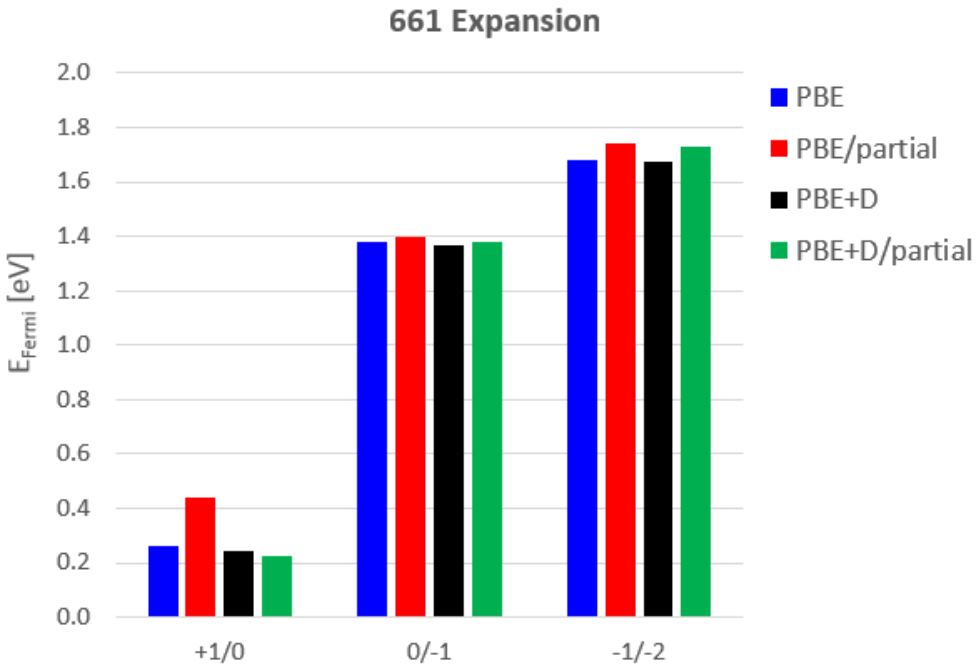

Fig. A-4 E_{Fermi} in eV for the *hh* divacancy defect in 4H-SiC at which transition between +1 and neutral (+1/0), neutral and –1 (0/–1), –1 and –2 (–1/–2) charge states occurs for the 661-cell expansion, PBE with and without D, and full and partial relaxation

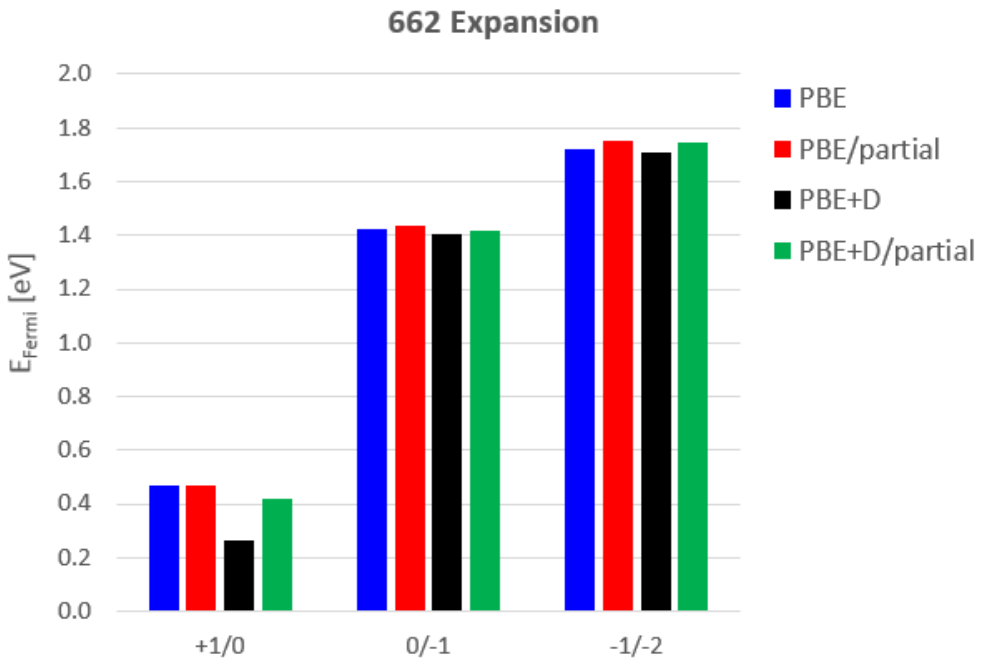

Fig. A-5 E_{Fermi} in eV for the *hh* divacancy defect in 4H-SiC at which transition between +1 and neutral (+1/0), neutral and –1 (0/–1), –1 and –2 (–1/–2) charge states occurs for the 662-cell expansion, PBE with and without D, and full and partial relaxation

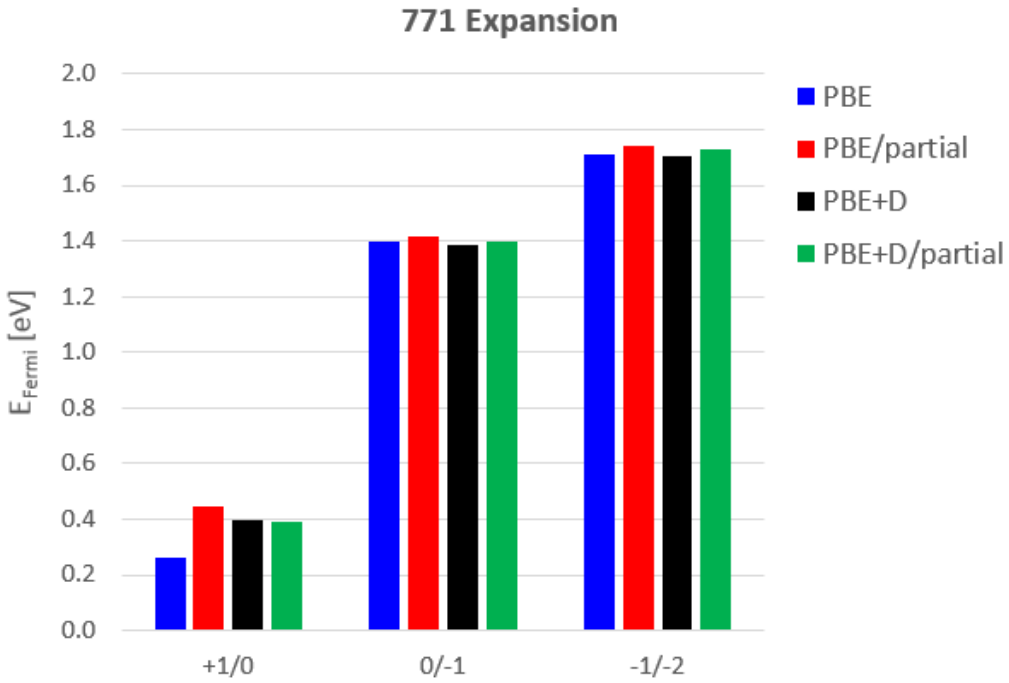

Fig. A-6 E_{Fermi} in eV for the *hh* divacancy defect in 4H-SiC at which transition between +1 and neutral (+1/0), neutral and –1 (0/–1), –1 and –2 (–1/–2) charge states occurs for the 771-cell expansion, PBE with and without D, and full and partial relaxation

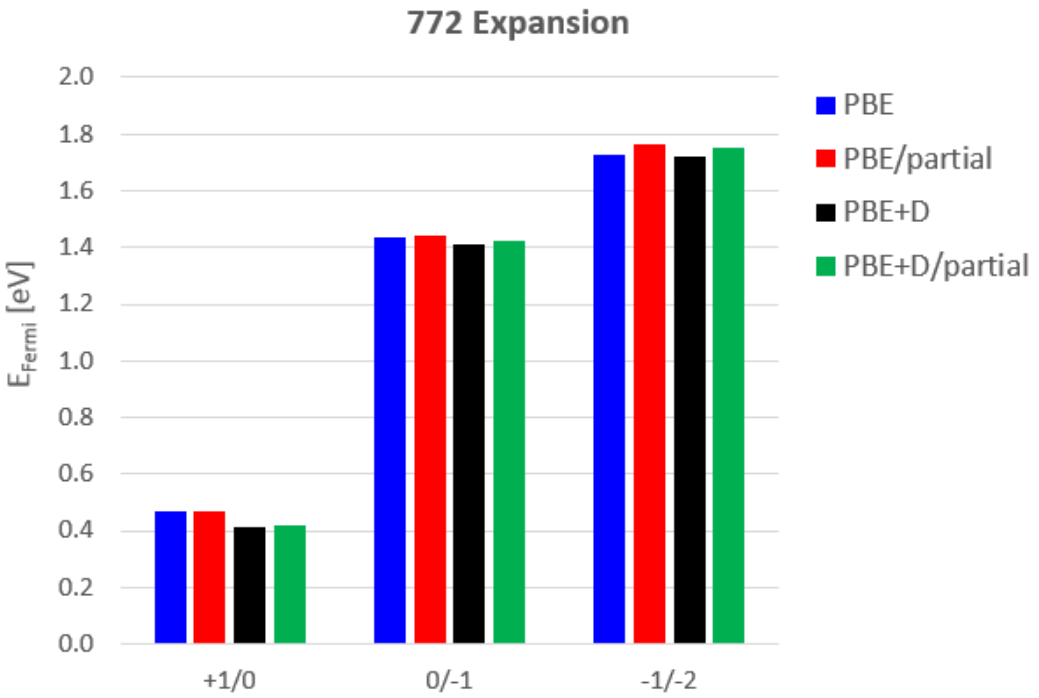

Fig. A-7 E_{Fermi} in eV for the *hh* divacancy defect in 4H-SiC at which transition between +1 and neutral (+1/0), neutral and –1 (0/–1), –1 and –2 (–1/–2) charge states occurs for the 772-cell expansion, PBE with and without D, and full and partial relaxation

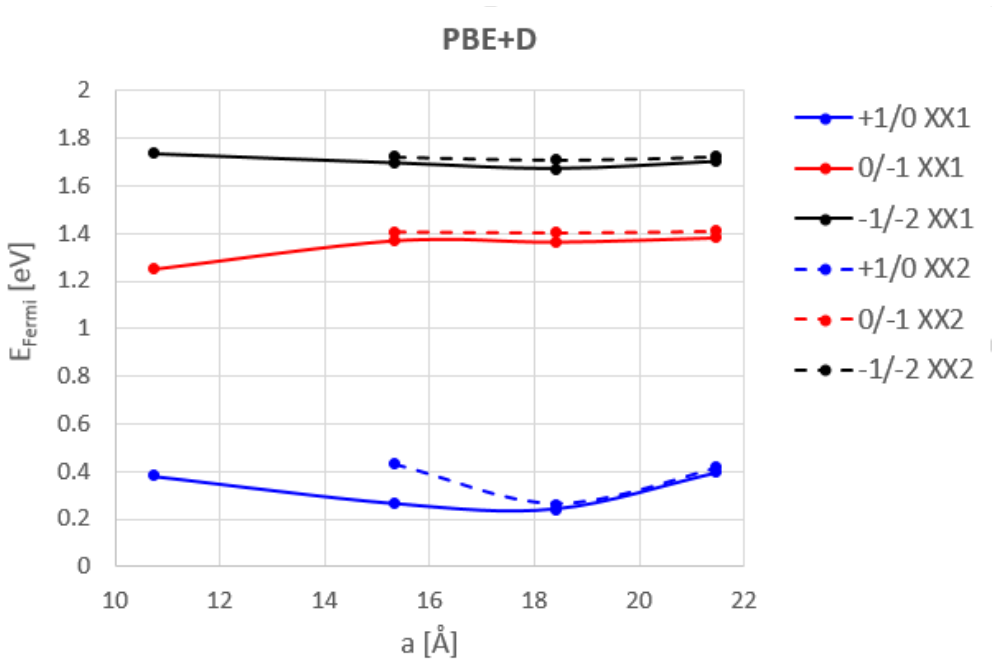

Fig. A-8 E_{Fermi} in eV for the *hh* divacancy defect in 4H-SiC at which transition between +1 and neutral (+1/0), neutral and –1 (0/–1), –1 and –2 (–1/–2) charge states occurs as a function of the cell parameter *a* in Å, PBE with D, and full relaxation

A.2 Zero Phonon Line

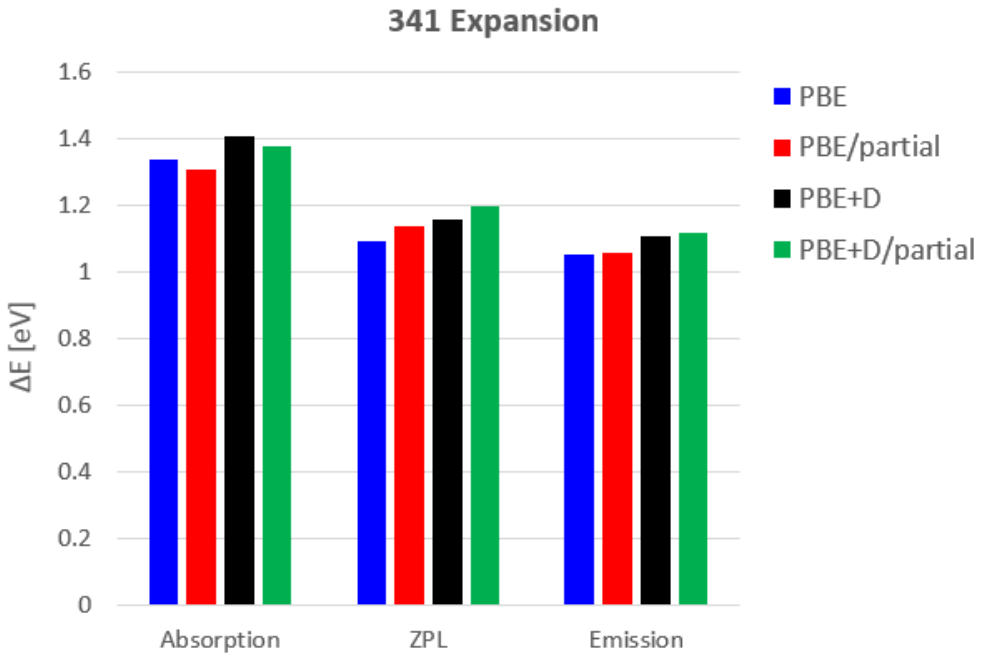

Fig. A-9 Absorption (Abs), zero phonon (ZPL), and emission (Em) lines in eV for the *hh* divacancy defect in 4H-SiC for the 341-cell expansion, PBE with and without D, and full and partial relaxation

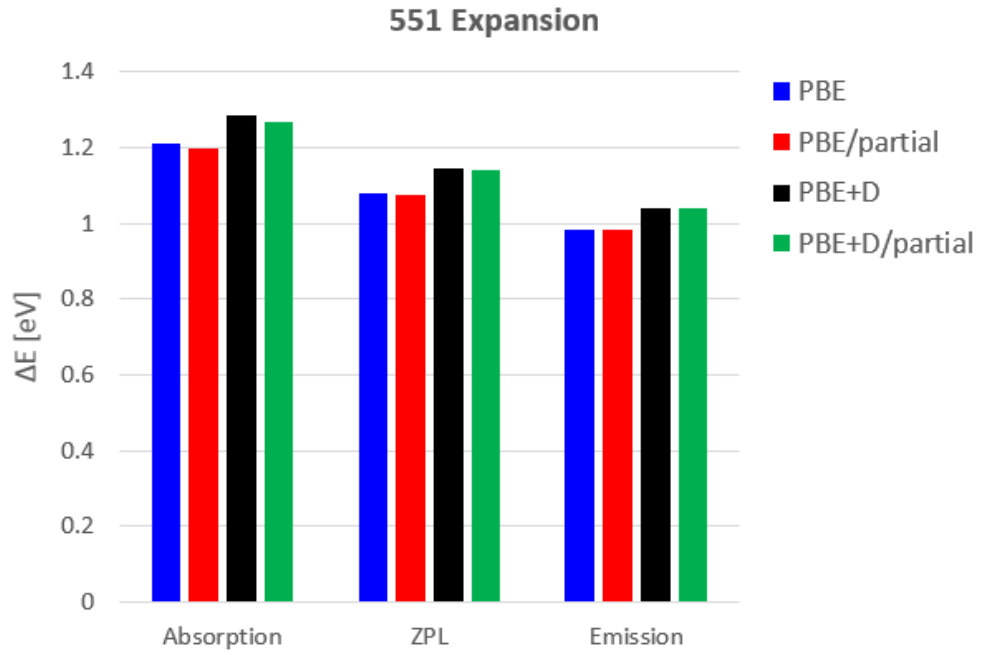

Fig. A-10 Abs, ZPL, and Em lines in eV for the *hh* divacancy defect in 4H-SiC for the 551-cell expansion, PBE with and without D, and full and partial relaxation

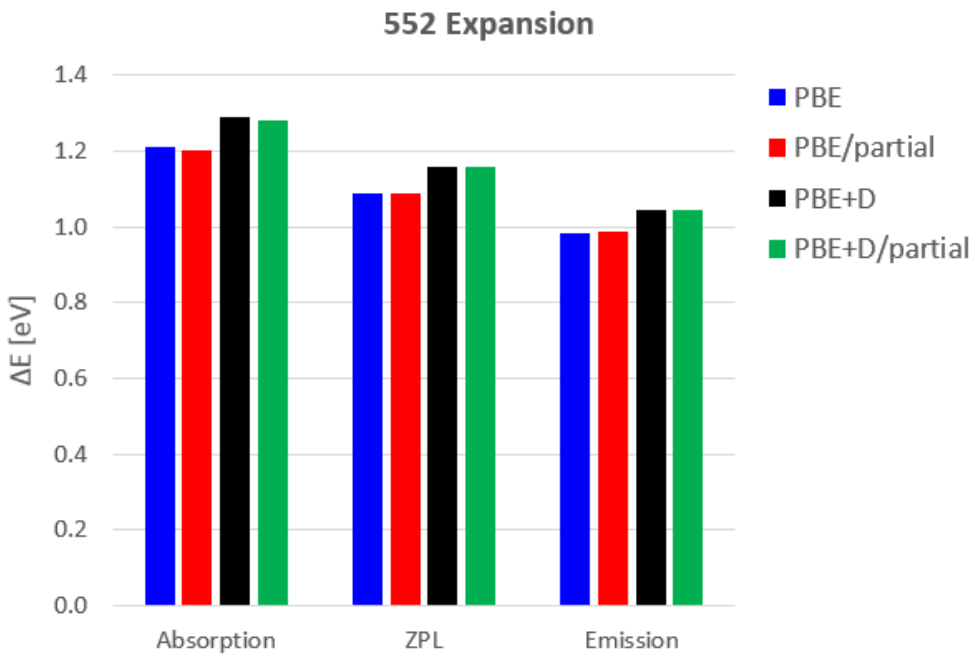

Fig. A-11 Abs, ZPL, and Em lines in eV for the *hh* divacancy defect in 4H-SiC for the 552-cell expansion, PBE with and without D, and full and partial relaxation

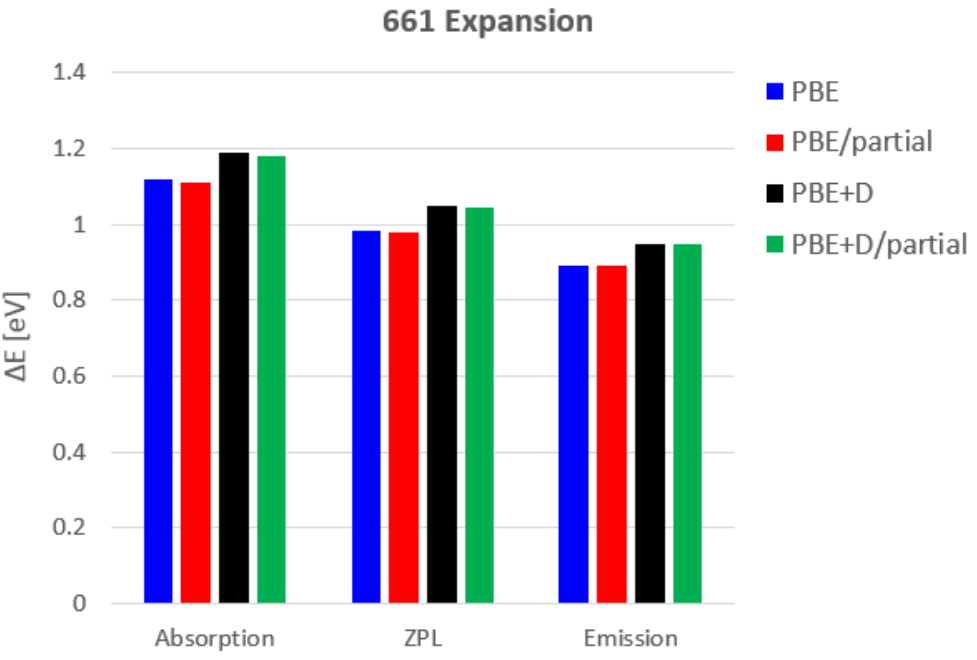

Fig. A-12 Abs, ZPL, and Em lines in eV for the *hh* divacancy defect in 4H-SiC for the 661-cell expansion, PBE with and without D, and full and partial relaxation

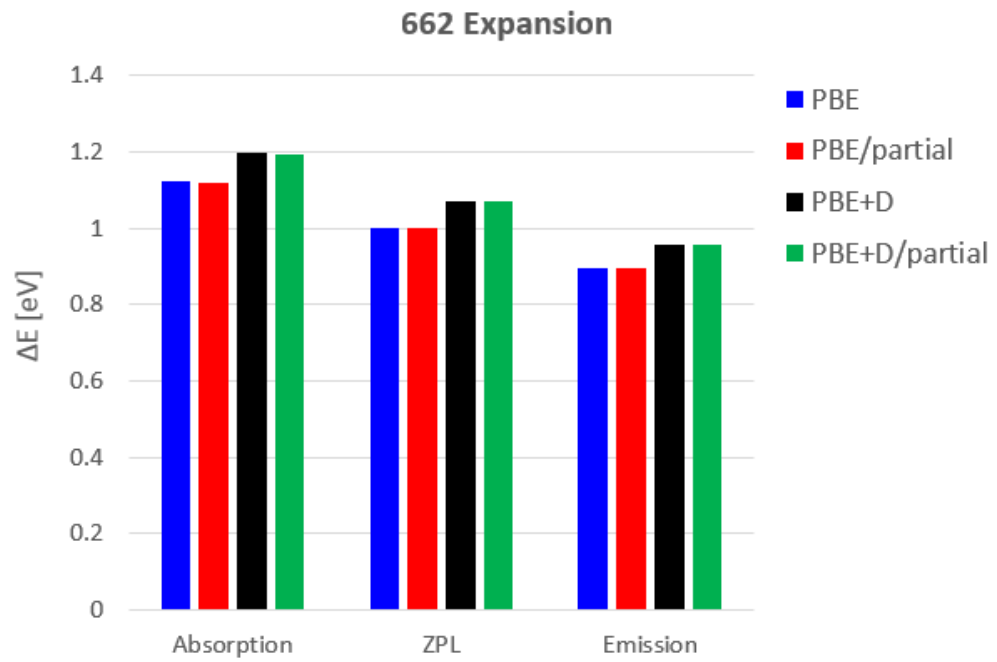

Fig. A-13 Abs, ZPL, and Em lines in eV for the *hh* divacancy defect in 4H-SiC for the 662-cell expansion, PBE with and without D, and full and partial relaxation

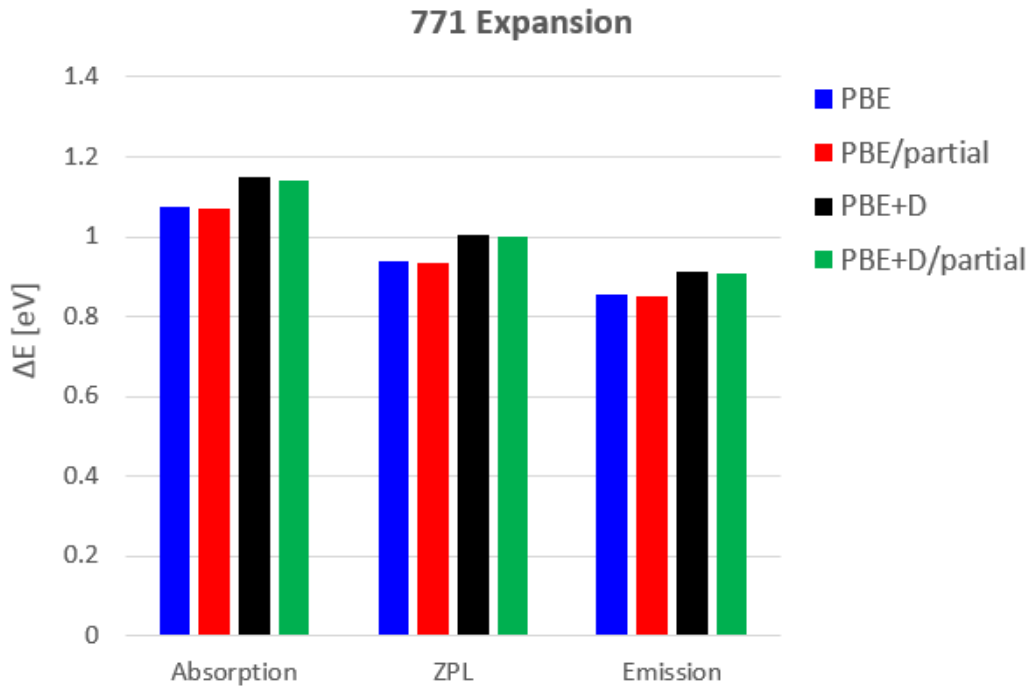

Fig. A-14 Abs, ZPL, and Em lines in eV for the *hh* divacancy defect in 4H-SiC for the 771-cell expansion, PBE with and without D, and full and partial relaxation

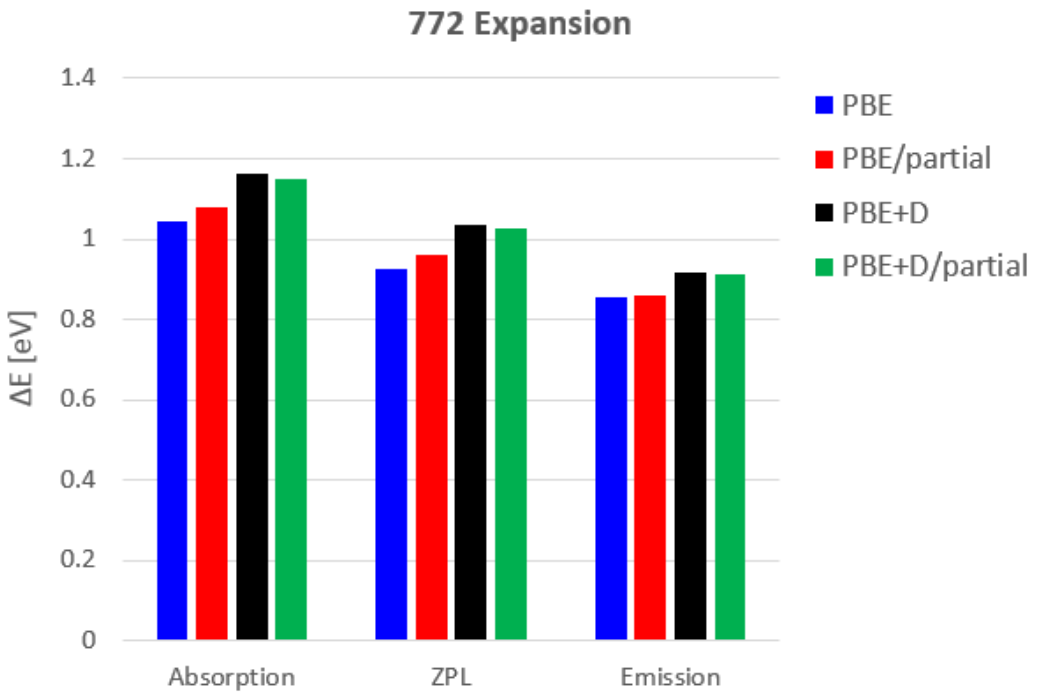

Fig. A-15 Abs, ZPL, and Em lines in eV for the *hh* divacancy defect in 4H-SiC for the 772 -cell expansion, PBE with and without D, and full and partial relaxation

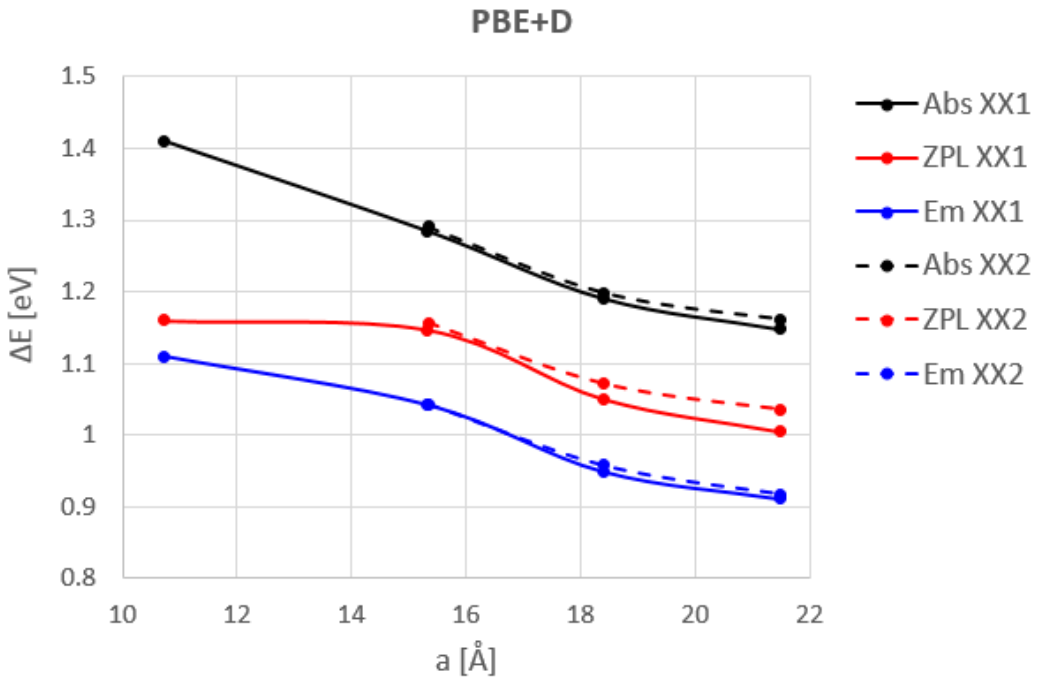

Fig. A-16 Abs, ZPL, and Em lines in eV for the *hh* divacancy defect in 4H-SiC as a function of the cell parameter *a* in Å, PBE with D, and full relaxation

INTENTIONALLY LEFT BLANK.

List of Symbols, Abbreviations, and Acronyms

Δε	bulk valence band maximum
Abs	absorption
D	dispersion
DFT	density functional theory
E_f	formation energy
E_{Fermi}	Fermi energy
Em	emission
eV	electronvolts
GGA	generalized gradient approximation
HSE	Heyd-Scuseria-Ernzerhof
IR	infrared
NV	nitrogen vacancy
PBE	Perdew-Burke-Ernzerhof
QE	Quantum Espresso
SiC	silicon carbide
XX1	expansion of x along *a*, 1 along *c*
XX2	expansion of x along *a*, 2 along *c*
ZPL	zero phonon line

1 (PDF) DEFENSE TECHNICAL INFORMATION CTR
DTIC OCA

2 (PDF) DIR ARL
IMAL HRA
RECORDS MGMT
RDRL DCL
TECH LIB

1 (PDF) GOVT PRINTG OFC
A MALHOTRA

1 (PDF) ARMY RSRCH OFFICE
J PARKER

22 (PDF) ARL
RDRL WM
B FORCH
RDRL WML
W OBERLE
RDRL WML B
N TRIVEDI
B RICE
E BYRD
W MATTSON
I BATYREV
B BARNES
J LARENTZOS
J BRENNAN
RDRL WML D
J VEALS
M MCQUAID
RDRL WMM B
E HERNANDEZ
RDRL WMM D
M TSCHOPP
RDRL WMM E
S COLEMAN
RDRL WMM G
J ANDZELM
C RINDERSPACHER
RDRL ROP
P REYNOLDS
RDRL SE
K SNAIL
M WRABACK
RDRL SEE Q
N FELL
RDRL SER E
M NEUPANE